

## Study of functional characteristics of mesoporous electrodes of supercapacitors based on silicon-carbon films

© I.Yu. Bogush, N.K. Plugotarenko, T.N. Myasoedova

Institute of Nanotechnologies, Electronics and Equipment Engineering, Southern Federal University,  
347928 Taganrog, Russia  
e-mail: inlys@sfedu.ru

Received July 3, 2022

Revised September 9, 2022

Accepted September 9, 2022

The study of the supercapacitor electrodes based on silicon-carbon films obtained by electrochemical deposition from solutions with different ratios of methanol/hexamethyldisilane and addition of manganese and nickel salts was carried out using cyclic voltammetry, electrochemical impedance spectroscopy and impedance Nyquist plots simulation by equivalent circuits method. The predominance of mesopores in the electrode samples was confirmed by the functional density method. According to a scanning electron microscopy study, the surface morphology of the silicon-carbon films is highly developed due to the presence of three-dimensional agglomerates and „foliated“ structures. The best retention of specific capacity after 450 charge/discharge cycles is observed for electrode samples containing manganese and nickel. Simulation of equivalent circuits showed that all types of electrodes have hierarchical pore structure. After 450 charge/discharge cycles an increase in pore storage resistance and a decrease in transport pore resistance due to the activation of deeper pore levels is observed. The applicability of Peukert's law for the electrodes based on silicon-carbon films for prediction of electrode discharge time is shown.

**Keywords:** Porous electrodes, silicon-carbon films, electrochemical impedance spectroscopy, equivalent circuit models, Peukert's law.

DOI: 10.21883/TP.2022.12.55195.175-22

### Introduction

Hybrid capacitors, also known as supercapacitors, are energy storage systems that attract attention by their very high power density, wide operating temperature range, and high number of charge/discharge cycles [1–4].

Highly porous carbon materials (activated carbon, carbon nanotubes, graphene) and film structures based on polyaniline [5–8] are widely used as electrodes for supercapacitors. In this regard, silicon-carbon films (SCF) [9] act as a promising material for supercapacitor electrodes.

Silicon-carbon films demonstrate the ability to store energy due to their electrical conductivity, long service life, high thermal and chemical stability in harsh physical and chemical environments [10,11]. Electrodes made from SCF can provide higher capacitance through a fast and reversible redox reaction [12,13]. Also, SCFs can be modified with metal atoms to achieve better electrode properties.

Carbon-based materials, commonly used as electrodes in supercapacitors, can be synthesized with a wide range of morphologies, which makes it possible to investigate the relationship between electrode material properties and electrochemical characteristics [14–16]. The porosity of the electrodes has a significant effect on their capacitive characteristics. Hierarchical porous materials containing micro-, meso- and macropores have improved characteristics for energy distribution and storage due to increased mass transfer through macropores and mesopores and maintenance of specific surface area at the level of micropores [17,18].

Impedance spectroscopy is used to interpret how electrode morphology can affect the capacitance characteristics of supercapacitors. Measuring the impedance of porous electrodes is a powerful tool for the design and characterization of electrodes, is widely used in practice, and can be studied by the equivalent circuit method [19]. Impedance models for porous electrodes can be divided into two types:

- 1) modeling of the hierarchical structure of pores, consisting of a multilevel system of charge accumulation and storage [20];
- 2) multiscale impedance model for porous electrodes with fractal structure [21].

In our paper, we assume that silicon-carbon electrodes have a hierarchical structure of pores of two types: transport pores and storage pores [20].

In previous papers [22,23] a number of properties was studied and the possibility of using SCFs obtained by electrochemical deposition according to the original method of the authors as electrodes of supercapacitors has been shown. The synthesized SCFs are porous materials that are interesting for applications in this area due to their structural characteristics [24,25].

The purpose of this paper was to study the effect of composition and porosity on the functional characteristics (capacity, stability, charge/discharge rate) of SCF-based electrodes, obtained by the electrochemical method from organic solutions of different compositions.

## 1. Materials and methods

### 1.1. SCF fabrication

„Pure“ SCF and SCF doped with metal atoms were obtained by the method of electrochemical deposition described in the papers [26,27]. The deposition was carried out on copper foil substrates  $28 \times 12 \times 0.5$  mm, mounted on the negative electrode. A plate made of pyrolytic graphite with a purity of 99.99% and dimensions  $4 \times 15 \times 25$  mm was used as a cathode. The electrochemical deposition of SCF was carried out in two stages: the first stage included the deposition of „pure“ SCF from solutions based on hexamethyldisilazane (HMDS) and methanol in a ratio of 1:1, 1:2 and 1:9 for 30 min at voltage 180 V. The second stage included introducing  $\text{Ni}(\text{NO}_3)_2 \cdot 6\text{H}_2\text{O}$  or  $\text{MnSO}_4 \cdot 5\text{H}_2\text{O}$  salts into the solution in the amount of 0.05 mass% and subsequent precipitation for 5 min at a potential of 40–60 V.

### 1.2. Material specifications

The morphology of the films was studied by scanning electron microscopy (SEM) using Nova NanoLab 600 equipment (FEI Company, the Netherlands). The specific surface area was determined by the BET technique and by the functional density method [28]. Isotherms for standard adsorption of  $\text{N}_2$  were measured using a Quantachrome Nova 2000E Surface Area setup (Quantachrome Instruments, USA). Samples with a weight of approximately 0.4 g were heated to  $200^\circ\text{C}$  in vacuum for at least 3 h to remove adsorption particles, after which  $\text{N}_2$  adsorption data were collected at relative pressures from 10 to 0.3 at 77 K (porosity measurements were carried out at the Collective Use Center of the Saratov State Technical University).

### 1.3. Electrochemical measurements and impedance modeling

Electrochemical characteristics were measured using Ellins P-45X potentiostat/galvanostat at room temperature in 8M NaOH solution. The study conditions do not contribute to the chemical degradation of the electrode material. The studies were carried out according to the three-electrode scheme. A commercial Ag/AgCl (3M KCl) electrode was used as a reference electrode, and a carbon electrode was used as a counter electrode.

The electrochemical characteristics of SCF were measured by cyclic voltammetry (CVA) at a scanning rate of 20–100 mV/s, galvanostatic charge-discharge at a current density of 430–860 mA/g, and electrochemical impedance spectroscopy in the frequency range from 0.01 Hz to 50 kHz. The characteristics were monitored at the beginning of measurements and after cycling.

Interpretation of the Nyquist plots was performed using the software ZView, Scribner Associates, designed to plot and analyze impedance data using the equivalent circuit method.

The total specific capacitance was estimated by cyclic voltammetry curves using the equation

$$C_m = \frac{I}{v \cdot m}, \quad (1)$$

where  $C_m$  is the specific capacitance, [F/g],  $I$  is the maximum cathode current, [A],  $m$  is the weight of deposited material, [g],  $v$  is the scanning speed, [V/s].

## 2. Results and discussions

### 2.1. SEM and porosity studies

The results of SCF surface morphology studies are shown in Fig. 1. It can be clearly observed in Fig. 1, *a* that „pure“ SCF, precipitated from a solution with a methanol:HMDS ratio of 1:1, has a „foliate“ morphology consisting of a set of needle-like set of nanolayers with minor inclusions of fine grains. The increase in the methanol portion in the solution to ratio of methanol:HMDS 2:1 in the solution leads to the partial destroying formation of the „foliated“ structure (Fig. 1, *b*). With an increase in the methanol portion to methanol:HMDS ratio of 9:1 (Fig. 1, *c*), the external morphology of the SCF completely changes and is characterized by the presence of three-dimensional spherical agglomerates. In the case of SCF doping with manganese (Fig. 1, *d*), one can see the growth of three-dimensional agglomerates, and the formation of acicular nanolayers. The surface of the Ni-containing SCF (Fig. 1, *e*) is probably coated with a nickel-containing phase, like the samples discussed in the earlier study, confirmed by Raman spectroscopy [23], and has a porous structure with grains and agglomerates. The thickness of the films measured by the interferometric method was in the range of 350–800 nm.

Analysis of SEM images showed that the synthesis conditions have an ambiguous effect on the surface morphology of the SCF samples; there are no evenly distributed pores, which size can be estimated. It is well known that electrode materials with higher specific surface area and pore size appropriate for a particular electrolyte can facilitate electron and ion transfer, which has a positive effect on the ability to store charge and can significantly speed up the actual use of supercapacitors [29,30]. Therefore, the investigation of  $\text{N}_2$  adsorption/desorption was used to study the specific surface area and pore size distribution of SCF. Fig. 2 shows that all the samples have a large number of mesopores. The size, volume of pores and specific surface area are shown in Table 1.

The highest specific surface area as per BET is observed for manganese-containing SCF, while the surface area of mesopores for manganese-containing SCF is obviously lower than that for nickel-containing and „pure“ SCF, which is explained by the formation agglomerates on the carbon surface, which „lock up“ part of the pores [30]. However, they can also increase the contact area between the electrode and electrolyte to improve functional

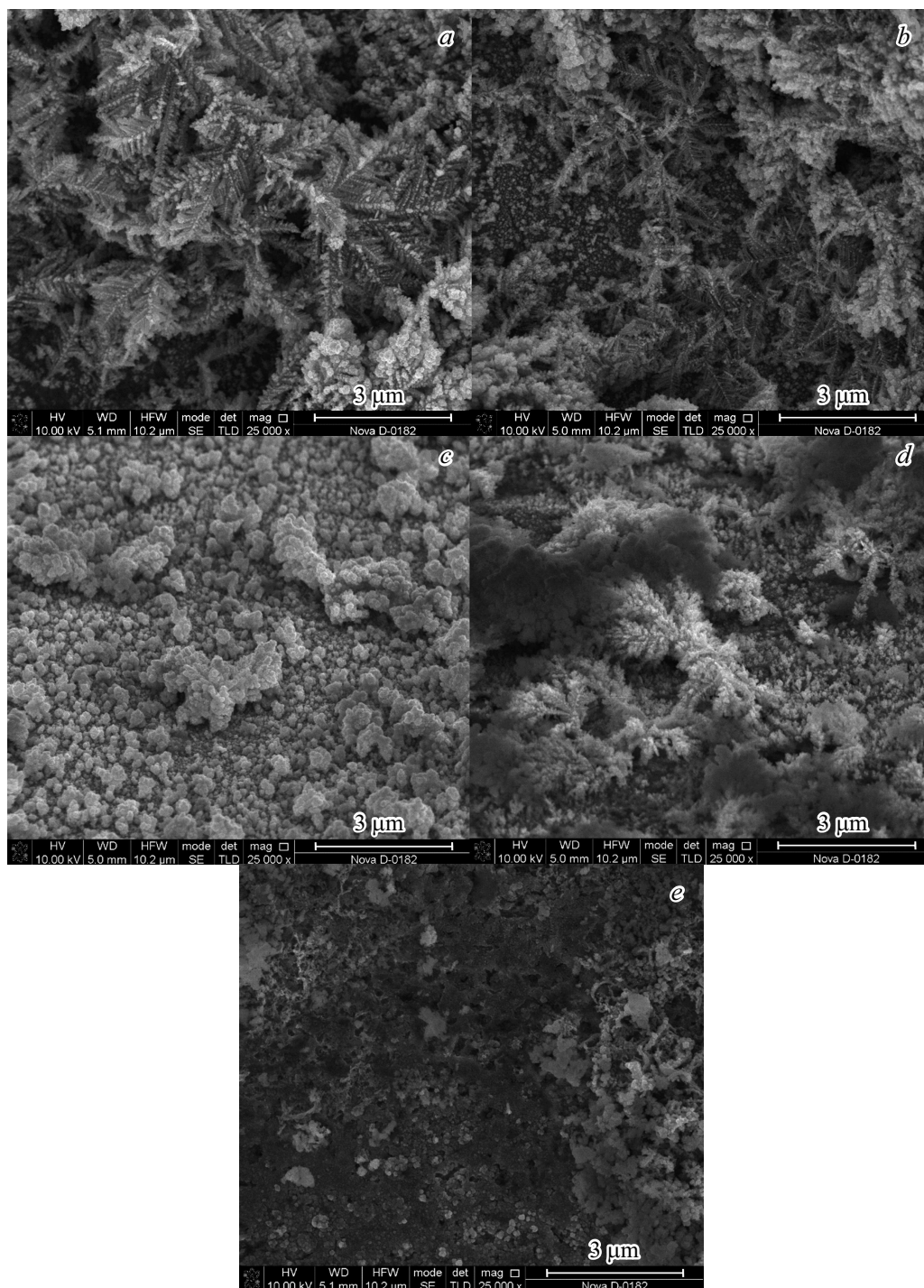


**Figure 1.** SEM images of SCFs obtained from solutions: *a* — methanol:HMDS 1:1; *b* — methanol:HMDS 2:1; *c* — methanol:HMDS 9:1; *d* — methanol-HMDS- $\text{Mn}^{2+}$ ; *e* — methanol-HMDS- $\text{Ni}^{2+}$ .

characteristics [31]. Ni-containing SCFs also have a high specific surface area (BET). The pore size distribution shows a bimodal pore distribution. This confirms that nickel, does not interact with the silicon-carbon matrix unlike manganese [23]. In the sample obtained from a solution based on methanol and HMDS with a ratio of 2:1, the highest value of the specific surface area of mesopores and micropores is observed.

## 2.2. Functional characteristics study and simulation

Fig. 3 shows the curves of cyclic voltammograms (CVAs) at a scanning rate of 20–100 mV/s with a potential window of 0–0.5 V. It is obvious that the shapes of the CVA curves do not show noticeable changes even at scan rate of 100 mV/s, confirming that the electrodes have a fast

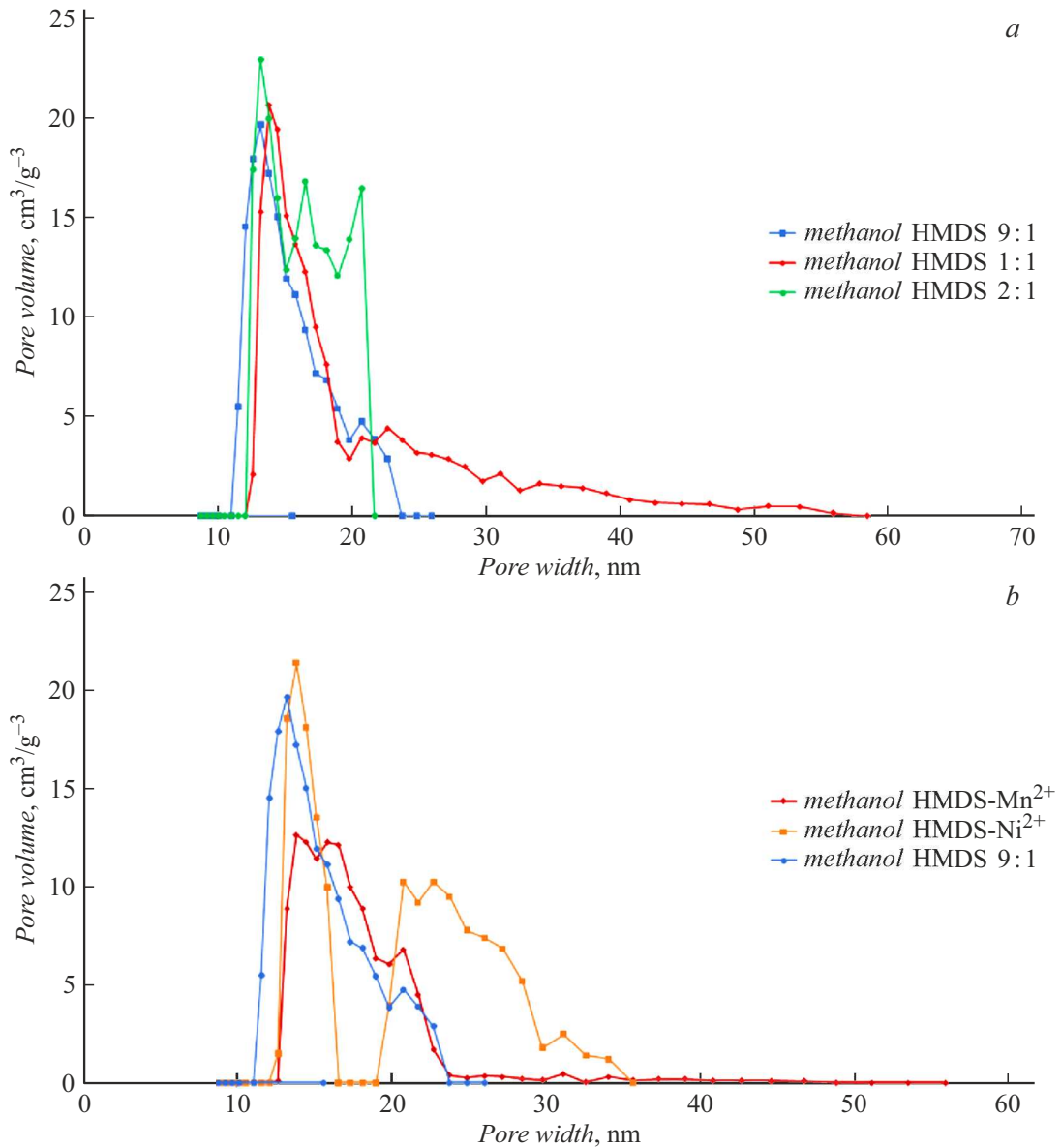


**Figure 2.** Distribution of mesopores by size of SCFs obtained from solutions: *a* — methanol-HMDS in ratios 1:1, 2:1, 9:1; *b* — methanol-HMDS in ratio 9:1 „pure“, with Ni<sup>2+</sup> added, with Mn<sup>2+</sup> added.

**Table 1.** Results of porosimetry analysis

Solution composition to get SRF	Specific area of surface, BET, m <sup>2</sup> g <sup>-3</sup>	Specific area of surface of mesopores, m <sup>2</sup> g <sup>-3</sup>	Average size of mesopores, nm	Pores volume, cm <sup>3</sup> /g	Specific area of surface of micropores, m <sup>2</sup> g <sup>-3</sup>	Average size of micropores, nm	Volume of micropores, cm <sup>3</sup> /g
Methanol:HMDS 1:1	133	72	58	1.36 · 10 <sup>-4</sup>	50	2	7.7 · 10 <sup>-5</sup>
Methanol:HMDS 2:1	134	83	22	1.37 · 10 <sup>-4</sup>	131	1.7	1.4 · 10 <sup>-4</sup>
Methanol:HMDS 9:1	118	69	26	1.04 · 10 <sup>-4</sup>	58	1.7	6 · 10 <sup>-5</sup>
Methanol-HMDS-Mn <sup>2+</sup>	165	51	56	8.758 · 10 <sup>-5</sup>	36	2.1	4.8 · 10 <sup>-5</sup>
Methanol-HMDS-Ni <sup>2+</sup>	150	70	36	1.43 · 10 <sup>-4</sup>	83	2	1.1 · 10 <sup>-4</sup>

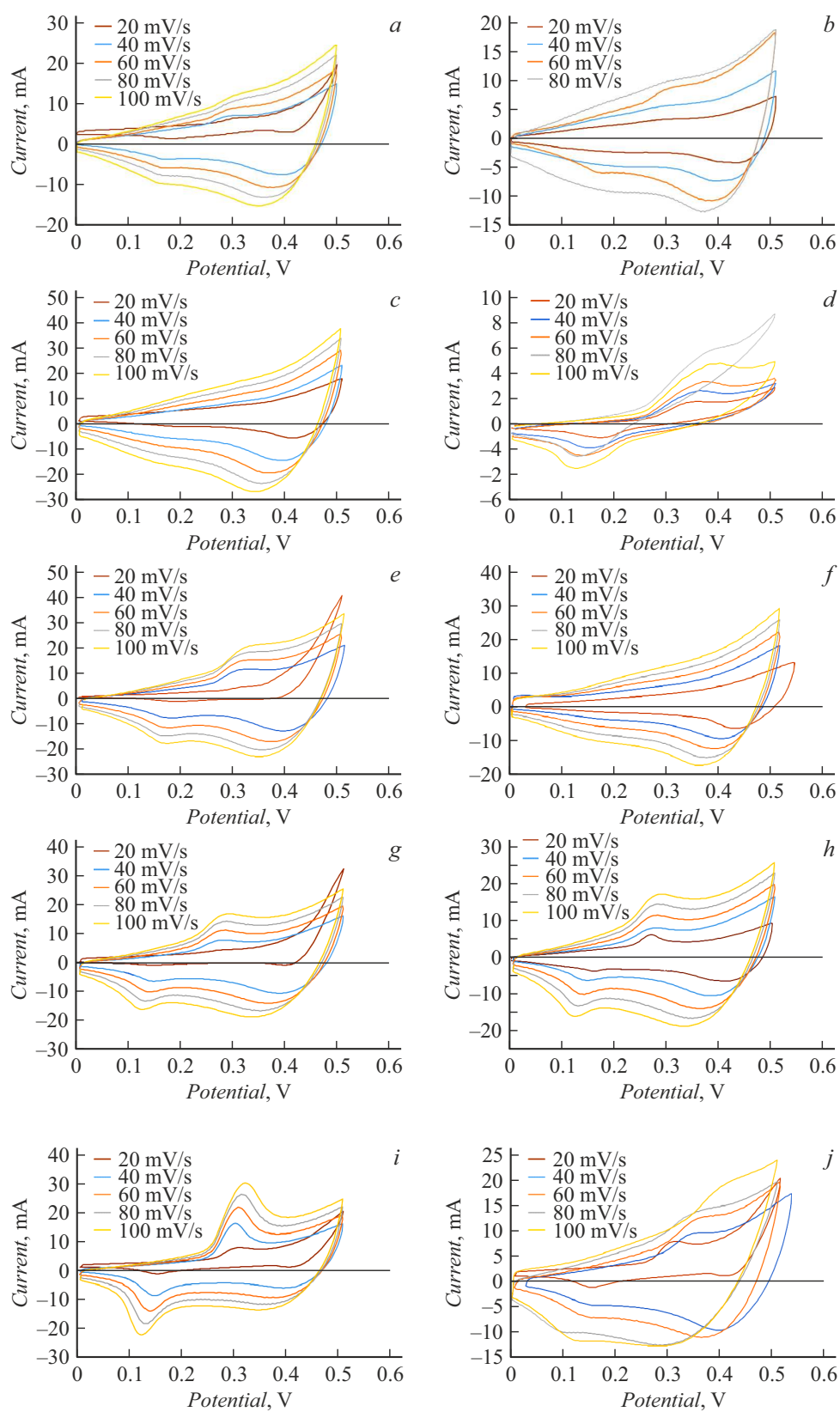


**Figure 3.** CVA of samples before and after 450 charge/discharge cycles for electrodes obtained from solutions: *a* — methanol:HMDS 1:1 before; *b* — methanol:HMDS 1:1 after; *c* — methanol:HMDS 2:1 before; *d* — methanol:HMDS 2:1 after; *e* — methanol:HMDS 9:1 before; *f* — methanol:HMDS 9:1 after; *g* — methanol:HMDS- $\text{Mn}^{2+}$  before; *h* — methanol:HMDS- $\text{Mn}^{2+}$  after; *i* — methanol:HMDS- $\text{Ni}^{2+}$  before; *j* — methanol:HMDS- $\text{Ni}^{2+}$  after.

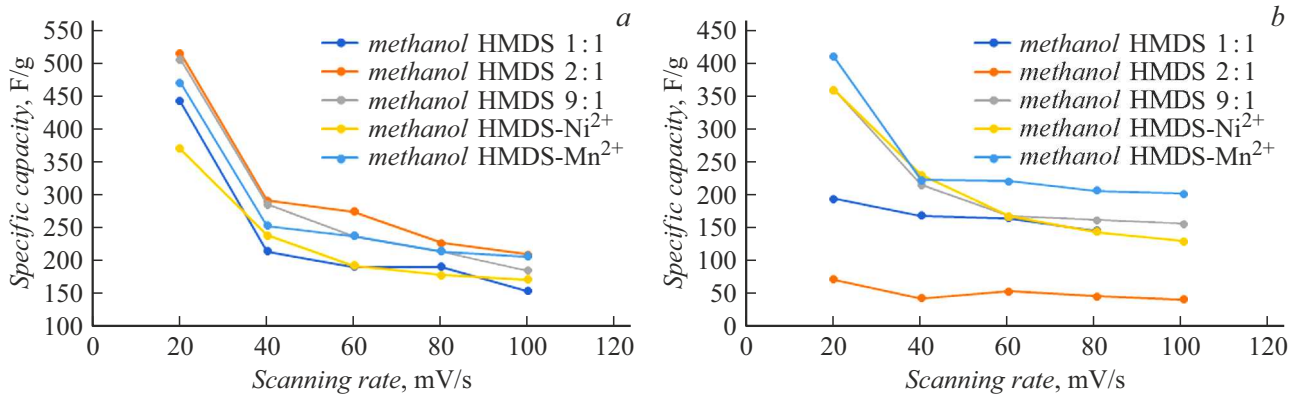
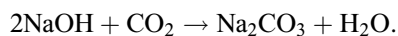


Figure 4. Specific capacity vs. scanning rate: *a* — before studies; *b* — after 450 charge/discharge cycles.

Table 2. Storage and retention of specific capacity

Composition of solution to receive SRF	Retention of specific capacity, %	Storage of specific capacity, %
Methanol:HMDS 1:1	79.6	70.9
Methanol:HMDS 2:1	81.4	17.4
Methanol:HMDS 9:1	79.1	74.85
Methanol-HMDS-Mn <sup>2+</sup>	83.6	86.62
Methanol-HMDS-Ni <sup>2+</sup>	83.5	91.6

charge transfer characteristic and a satisfactory rate. For all samples redox peaks are observed as a result of a reversible redox reaction that occurs on the surface of the electrode materials. For „pure“ SCF the peaks are almost unnoticeable, while the height of the peak increases with the metals introduction into the film, especially in the sample with the nickel addition. The reaction mechanism can be represented by the following scheme [23]:



To understand the mechanisms of charge storage, exponential analysis was carried out at a potential of 0.5 V [32]:

$$i(v) = av^\beta, \quad (2)$$

where  $i$ ,  $v$ ,  $a$  and  $\beta$  are current density, scan rate, and arbitrary constants, respectively. The value  $\beta$  has two well-defined conditions:  $\beta = 0.5$  indicates a general diffusion-controlled process of Faraday reactions on the electrode surface, and  $\beta = 1.0$  indicates that the charge storage process is capacitive. For the samples under study the calculated average value  $\beta$  varies from 0.75 to 0.97, thus, the contribution to the capacitive charge accumulation prevails, since  $\beta$  is close to one [21].

The specific capacity values before and after cycling were estimated from the CVA curves (Fig. 4) using equation (1).

The highest specific capacity before study is observed in films obtained from solutions based on methanol and HMDS with ratio of 2:1. It decreases from 516 to 209 F/g. (retention 81.4%). For Mn-containing SCFs the specific capacitance decreases from 471 to 207 F/g (retention 83.6%) during scanning rate decreases from 20 to 100 mV/s, which indicates a good rate capability of the films under study. Subsequently, the cycling characteristics of the electrodes were tested after 450 charge/discharge cycles, as shown in Fig. 4, *b* (see also Table 2). The specific capacity retention for Mn-containing and Ni-containing SCFs is 86.62% and 91.6%, respectively. This confirms that the porous structure has good cyclic stability [32]. At the same time, the specific capacitance for the sample obtained from a solution based on methanol and HMDS with ratio of 2:1 reduces significantly to 17.4% after the cycling due to the fact that in this type of electrodes the microporous structure prevails, which is destroyed during the electrode operation [33].

The charge/discharge curves of mesoporous SCFs at different current densities are shown in Fig. 5. The charge/discharge time is significantly longer for the sample prepared from the solution of methanol and HMDS with ratio 2:1, what proved by the higher specific capacitance and larger pore volume. The discharge curves of the SCF are non-linear, which confirms their pseudocapacitive nature. In the case of SCFs doped with manganese and nickel the presence of noticeable plateau (especially in the case of nickel) on the discharge curve indicates the occurrence of redox reactions in accordance with the CVA curves [27]. For „pure“ SCF, there are no noticeable plateaus, which indicates that the primary process is the discharge of a double electric layer formed on the surface of the material during charging.

The effect of the physical properties of supercapacitor electrodes on the delivered charge was carried out using Peukert's law. [34]. This empirical law states that the delivered battery charge depends on the discharge current: the greater the discharge current is, the less the delivered charge is, since  $k > 1$ :

$$Q = I^k t, \quad (3)$$

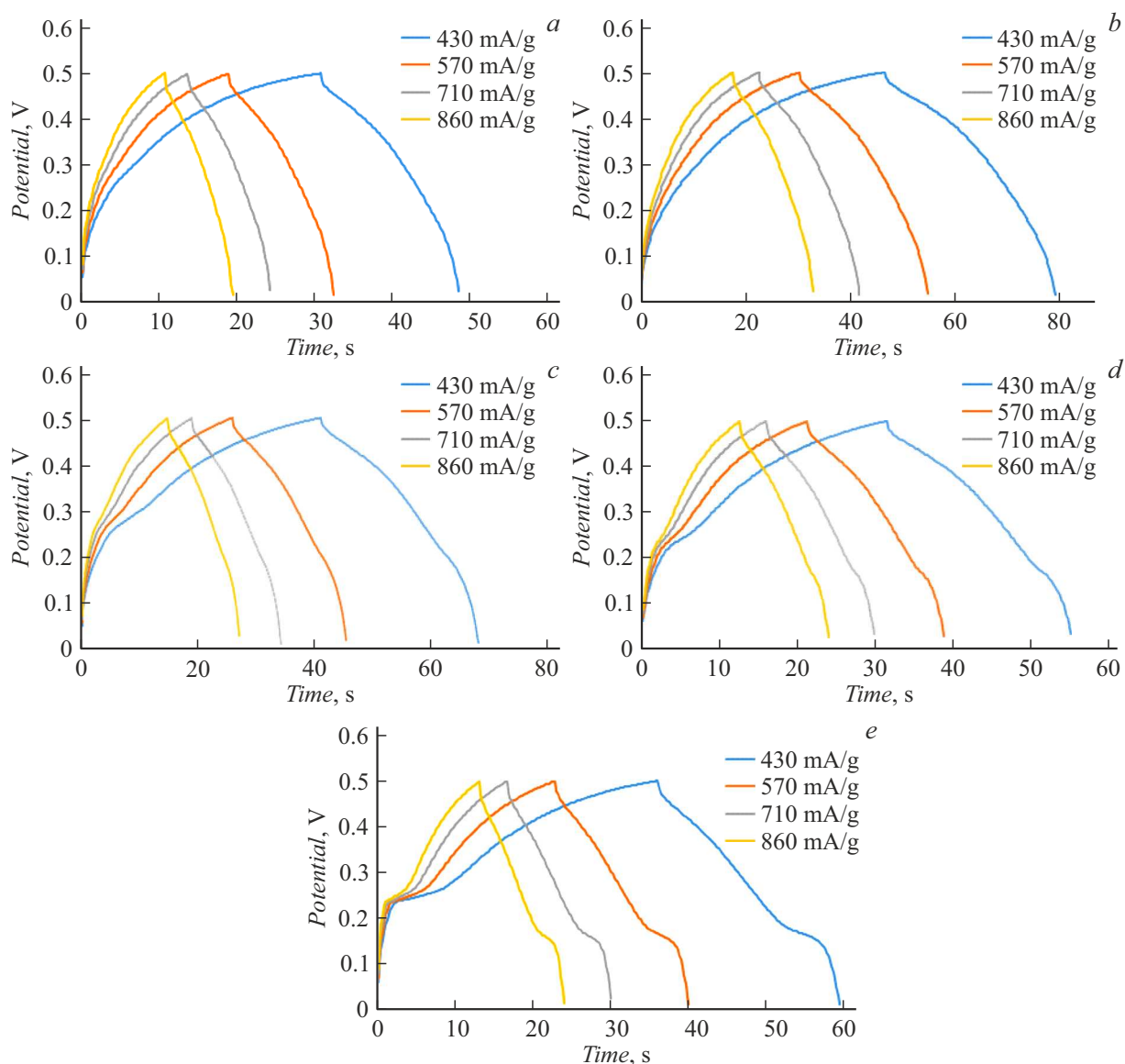


**Figure 5.** Charge/discharge curves at different current densities for electrodes obtained from their solutions: *a* — methanol:HMDS 1:1; *b* — methanol:HMDS 2:1; *c* — methanol:HMDS 9:1; *d* — methanol-HMDS- $\text{Mn}^{2+}$ ; *e* — methanol-HMDS- $\text{Ni}^{2+}$ .

where  $Q$  is the delivered charge,  $I$  is the discharge current,  $t$  is the discharge time,  $k$  is the Peukert's constant, which is dimensionless and empirical.

The relationship between the discharge current and the delivered charge for the samples under study is shown in Fig. 6.

It can be seen from Fig. 6, *a* that the application of Peukert's law for this case is justified, since the ratio between the delivered charge and the discharge current is the same for all samples: the delivered charge increases with a decrease in the discharge current. This pattern is explained by the laws of macrokinetics and can be due to the combined effect of three aspects of the physics of electrodes: the structure of the porous electrode, charge redistribution, and self-discharge.

From this it follows that the discharge time of the electrodes can be predicted using the equation. To predict the electrode discharge time equation (3) is as follows:

$$t = Q/I^k. \quad (4)$$

Fig. 6, *b* shows the experimental and predicted discharge times. Approximation confidence factor  $R^2$  for all cases was minimum 0.99, which indicates the best fit of the predicted data. The value of the relative error of the predicted data is maximum 3%, which is sufficient for practical calculations. The obtained values of the Peukert constant are presented in Table 3. Values  $k$  are greater than one indicating that the capacitance will decrease with the current increasing.

From Table 3 data it can be seen that the Peukert constant for samples with a larger specific surface area of mesopores

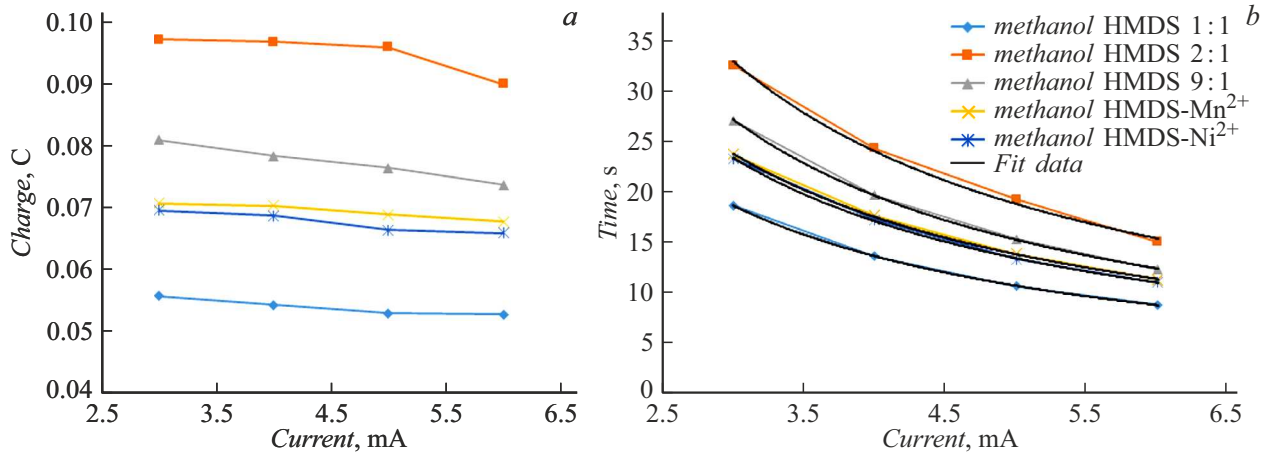


**Figure 6.** Ratio between delivered charge and discharge current (a); experimental and predictive discharge curves (b).

**Table 3.** Determination of the Peukert constant for electrode samples

The composition of the solution for obtaining SCF	$k$
Methanol:HMDS 1:1	1.095
Methanol:HMDS 2:1	1.130
Methanol:HMDS 9:1	1.084
Methanol-HMDS-Mn <sup>2+</sup>	1.063
Methanol-HMDS-Ni <sup>2+</sup>	1.083

(Table 1) is slightly higher, which also indicates that these types of electrodes have a more porous structure [34].

To study the impedance of mesoporous electrodes, the experiments were carried out to measure the spectra of electrochemical impedance (EIS). It is important to note that we measured the characteristics before and after 450 charge/discharge cycles. This made it possible to study the effect of pores activation on the measured electrode impedance.

Figure 7 shows the results of EIS for the studied electrode samples. Predominantly linear Nyquist plots without a semicircle in the high frequency region show that the charge transfer of these work electrodes is sufficient for applications in supercapacitors. The low frequency portion of the Nyquist plots shows deviation from the vertical line, which is the result of non-ideal capacitive behavior [35] due to the porosity of the films. From the profiles of the Nyquist plots after 450 cycles for Mn-containing and Ni-containing SCFs in the high-frequency region one can observe a semicircle followed by a straight line with a phase angle  $\sim 45^\circ$ , which is consistent with the theory of hierarchical porosity, proposed in the paper [36]. For „pure“ SCF samples obtained from solutions with a ratio of methanol:HMDS 2:1, after 450 discharge cycles the inductance is observed, which can be explained by the influence of a thin side layer of charge/discharge reactions [37].

For further interpretation of the electrode characteristics the EIS data were compared with the proposed linear model of the electrochemical impedance considered in the paper [36]. This model (Fig. 7, insert) assumes that porous electrodes have two types of pores: „transport pores“ and  $R_s$  — cell internal resistance associated with the reaction at the electrode/electrolyte interface,  $Cdl$  — capacity of the electric double layer,  $Rdl$  — charge transfer resistance.  $Wt$  — open Warburg element responsible for resistance ( $Wt-Rt$ ) and capacity ( $Wt-Ct$ ) of transport pores,  $Ws$  — open Warburg element responsible for resistance ( $Ws-Rs$ ) and capacity ( $Ws-Cs$ ) of storage pores.

The calculated model parameters are presented in Table 4.

According to the simulation results, noticeable changes in the charge transfer resistance were observed.  $Rdl$  for all samples decreases significantly as the number of cycles increases. This behavior is explained by the kinetics of adsorbed ions during the formation of outer/inner layers of the electrical double layer [38]. Besides, the capacity also decreases as the number of charge cycles increases. This is mainly caused by the acceleration of adsorption reactions and by the rate of diffusion caused by a large differential potential [39]. The capacity of the electrical double layer for samples prepared from solutions based on methanol and HMDS with ratio of 2:1, and samples with the addition of manganese and nickel is much higher, this is consistent with the larger surface area of the samples, as well as a large pore volume (Table 1). For the sample based on methanol and HMDS 2:1, the capacity of the electric double layer changes insignificantly after 450 charge-discharge cycles, which is confirmed by the relatively stable EIS plots (Fig. 7, b).

According to Table 4 it can be concluded that the measured impedance of the samples before the study demonstrates characteristics with a fairly low „storage“ pore resistance ( $R_s$  is by 4 times less than  $R_t$ ), while after 450 charge/discharge cycles there is increase in the resistance of the „storage“ pores and decrease in the resistance in the „transport“ pores observes, which is

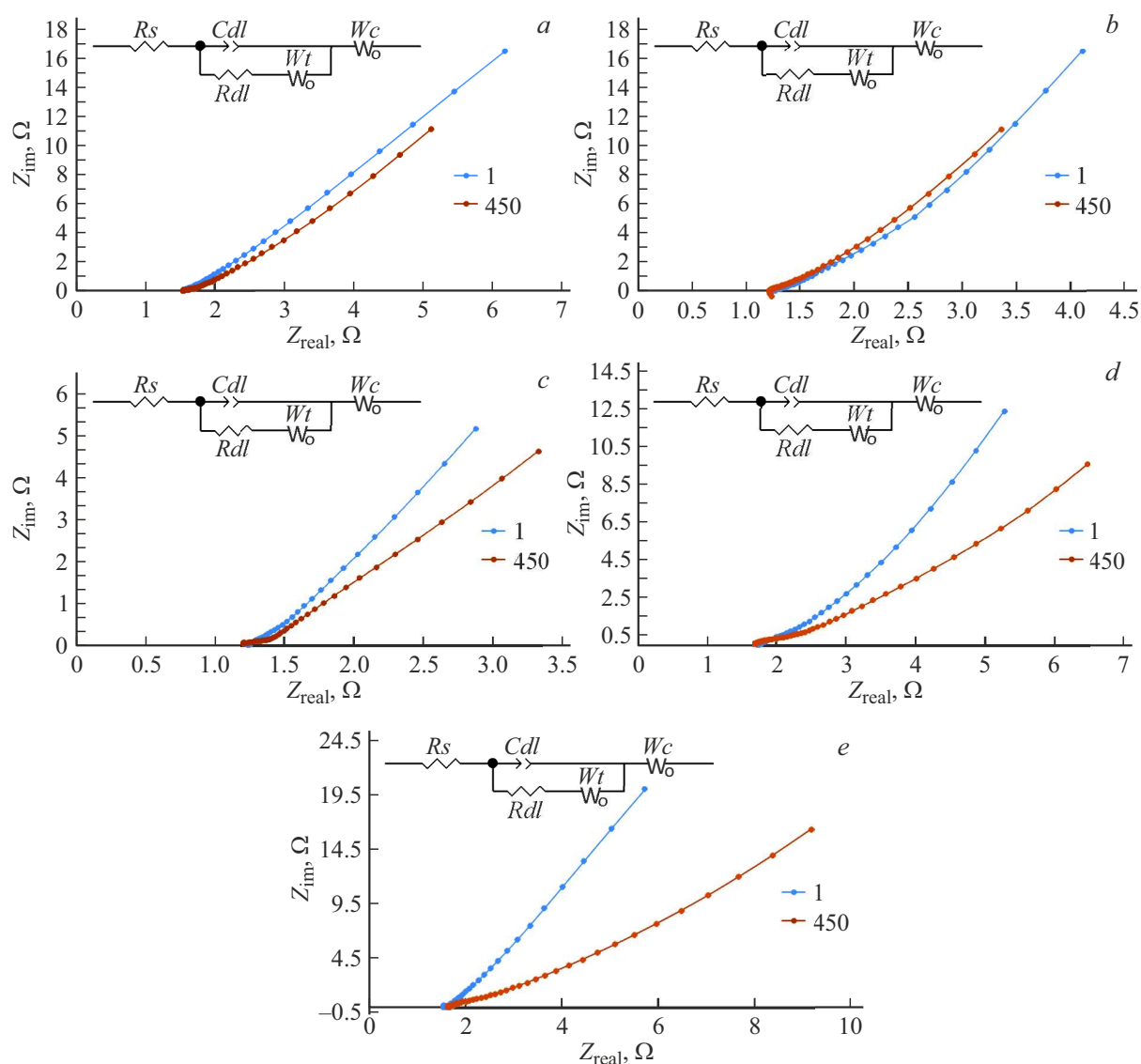


**Figure 7.** Nyquist plots recorded for electrodes obtained from the following solutions: *a* — methanol:HMDS 1:1; *b* — methanol:HMDS 2:1; *c* — methanol:HMDS 9:1; *d* — methanol-HMDS-Mn<sup>2+</sup>; *e* — methanol-HMDS-Ni<sup>2+</sup>.

**Table 4.** Model parameters for equivalent circuits

Composition of solution for obtaining SCF	Number of cycles	$R_s, \Omega$	$Cdl, F^{-3}$	$Rdl, \Omega$	$Wt-Rt, \Omega$	$Wt-Ct, F^{-3}$	$Ws-Rs, \Omega$	$Ws-Cs, F^{-5}$
Methanol:HMDS 1:1	1	1.549	7.8	1.012	7.02	15	0.00015	2.7
Methanol:HMDS 1:1	450	1.53	1.7	0.88	0.70	3.1	0.0024	42
Methanol:HMDS 2:1	1	1.247	91	6.47	4.52	34	0.0019	3.3
Methanol:HMDS 2:1	450	1.228	82	3.97	1.27	16	0.0035	23
Methanol:HMDS 9:1	1	1.543	48	1.21	5.15	9.1	0.00016	5.7
Methanol:HMDS 9:1	450	1.52	58	1.16	0.66	6.3	0.0024	42
Methanol-HMDS-Mn <sup>2+</sup>	1	1.74	76	4.095	48.2	108	0.0022	6.8
Methanol-HMDS-Mn <sup>2+</sup> 450	1.629	23	3.582	32.5	105	0.0049	18	
Methanol-HMDS-Ni <sup>2+</sup>	1	1.571	63	3.78	22.4	13	0.000206	5.8
Methanol-HMDS-Ni <sup>2+</sup>	450	1.608	14	0.89	7.33	22	0.00074	12

explained by the activation of deeper levels of the pores [40]. Secondly, the resistance of „transport“ pores is mainly responsible for the migration of electrolyte ions into the porous structure. For „pure“ SCFs the lowest transport pore resistance value ( $5.15 \Omega$ ) was determined, clearly demonstrating the beneficial contribution of its large surface area and mesoporosity to ensure proper ion migration and accessibility. The high resistance obtained for Ni-containing SCF ( $22.41 \Omega$ ), despite the approximately equal surface area, is consistent with the bimodal pore distribution (Fig. 2). The addition of manganese also resulted in high „transport“ pore resistances ( $48.29 \Omega$ ), consistent with the larger surface area.

Simulation results also showed an increase in „storage“ pore resistance by approximately 85.6% for all samples. These data indicate that as the number of charge/discharge cycles increases, a significant number of new nanometer features (new storage pores) [38] are activated.

The simulation data and experimental data are in good agreement, the approximation confidence factor  $R^2$  for all electrodes is more than 0.98, which indicates the validity of the selected equivalent circuit.

## Conclusion

Electrodes based on SCF, obtained from solutions of methanol and HMDS with ratio of 2:1, have the largest surface area of mesopores and micropores determined by the functional density method, but the high specific capacity of such electrodes is not maintained during the electrode operation, which may be due to destruction of the micropore structures. For electrodes based on Ni-containing SCF, showing a bimodal pore distribution, the retention of specific capacitance is maximum. The highest BET specific surface area was found in manganese-containing SCF. For this type of electrodes it is possible to predict the electrode discharge time according to the Peukert law.

Simulation of Nyquist plots by the equivalent circuit method showed that all types of electrodes are described by a single electrical circuit and have hierarchical pore structure. During the electrodes operation after 450 charge/discharge cycles deeper storage pores are activated, which leads to increase in the storage pores resistance by 85.6%. Nyquist plots show that the charge transfer of these electrodes is sufficient for applications in supercapacitors.

Thus, the studies performed shown that decrease in the ratio of methanol and HMDS in solution during the SCF production by electrochemical deposition leads to porous structure, which is destroyed during the electrode operation. The most promising for creating supercapacitor electrodes are nickel-containing SCFs, which are characterized by a bimodal pore distribution and retain their capacity for a long number of charge/discharge cycles.

## Funding

The research was supported by the Strategic Academic Leadership Program of the Southern Federal University („Priority 2030“).

## Conflict of interest

The authors declare that they have no conflict of interest.

## References

- [1] M.J. Chen, J.Y. Wang, H.J. Tang, Y. Yang, B. Wang, H.J. Zhao, D. Wang. *Inorg. Chem. Front.*, **3**, 1065 (2016). DOI: 10.1039/C6QI00083E
- [2] J. Li, G. Zhang, C. Fu, L. Deng, R. Sun, C.-P. Wong. *J. Power Sources*, **345**, 146 (2017).
- [3] K. Parida, V. Bhavanasi, V. Kumar, J. Wang, P.S. Lee. *J. Power Sources*, **342**, 70 (2017).
- [4] X.X. Zhao, R.B. Yu, H.J. Tang, D. Mao, J. Qi, B. Wang, Yu Zhang, H. Zhao, W. Hu, D. Wang. *Adv. Mater.*, **29**, 1700550 (2017). DOI: 10.1002/adma.201700550
- [5] H. Zhuang, N. Yang, L. Zhang, R. Fuchs, X. Jiang. *ACS Appl. Mater. Interfaces*, **7** (20), 10886 (2015). DOI: 10.1021/acsami.5b02024
- [6] D.K. Basa, G. Ambrosone, U. Coscia, A. Setaro. *Appl. Surf. Sci.*, **255**, 5528 (2009). DOI: 10.1016/j.apsusc.2008.09.042
- [7] T. Qin, Z. Wan, Z. Wang, Y. Wen, M. Liu, S. Peng, D. He, J. Hou, F. Huang, G. Cao. *J. Power Sources*, **336**, 455 (2016). DOI: 10.1016/j.jpowsour.2016.11.003
- [8] D.-H. Liu, W.-H. Li, H.-J. Liang, H.-Y. Lü, J.-Z. Guo, J. Wang, X.-L. Wu. *J. Mater. Chem. A*, **6**, 15797 (2018).
- [9] P. Zhou, L. Chen, M. Zhang, Q. Huang, C. Cui, X. Li, L. Wang, L. Li, C. Yang, Y. Li. *J. Alloys Compd.*, **797**, 826 (2019).
- [10] Y. Zhao, W. Kang, L. Li, G. Yan, X. Wang, X. Zhuang, B. Cheng. *Electrochim. Acta.*, **207**, 257 (2016). DOI: 10.1016/j.electacta.2016.05.003
- [11] C.B. Amara, H. Hammami, S. Fakhfakh, A. Kallel. *J. Electron. Mater.*, **50** (10), 5915 (2021). DOI: 10.1007/s11664-021-09129-7
- [12] F. Naseri, S. Karimi, E. Farjah, E. Schaltz. *Renew. Sust. Energ. Rev.*, **155**, 111913 (2022). DOI: 10.1016/j.rser.2021.111913
- [13] X.B. Yan, B.K. Tay, G. Chen, S.R. Electrochem. Commun., **8** (5), 734 (2006).
- [14] H. Zhuang, N. Yang, L. Zhang, R. Fuchs, X. Jiang. *Appl. Mater. Int.*, **7** (20), 10886 (2015).
- [15] C.-H. Chang, B. Hsia, J.P. Alper, S. Wang, L.E. Luna, C. Carraro, S.-Y. Lu, R. Maboudian. *ACS Appl. Mater. Int.*, **7** (48), 26658 (2015).
- [16] X.-Z. Ding, B.K. Tay, S.P. Lau, P. Zhang, X.T. Zeng. *ARC Thin Solid Films*, **408** (1–2), 183 (2002).
- [17] D. Gruet, B. Delobel, D. Sicsic, I.T. Lucas, V. Vivier. *Electrochim. Acta*, **295**, 787 (2019). DOI: 10.1016/j.electacta.2018.10.115
- [18] Q.-A. Huang, Yu Li, K.-Ch. Tsay, Ch. Sun, Ch. Yang, L. Zhang, J. Zhang. *J. Power Sources*, **400**, 69 (2018). DOI: 10.1016/j.jpowsour.2018.07.108
- [19] M.-L. Tremblay, M.H. Martin, C. Lebouin, A. Lasia, D. Guay. *Electrochim. Acta*, **55** (21), 6283 (2010). DOI: 10.1016/j.electacta.2009.11.006

- [20] I.A. Markevich, G.E. Selyutin, N.A. Drokin. *Tech. Phys.*, **64** (9), 1324 (2019). DOI: 10.1134/S1063784219090093
- [21] A.A. Nechitailov, N.V. Glebova, A.A. Tomasov, A. Krasnova, N.K. Zelenina. *Tech. Phys.*, **64** (6), 839 (2019). DOI: 10.1134/S1063784219060136
- [22] N.K. Plugotarenko, T.N. Myasoedova, I.Y. Bogush. *Mater. Sci. Semicond. Process.*, **135**, 106121 (2021). DOI: 10.1016/j.mssp.2021.106121
- [23] T.N. Myasoedova, M.N. Grigoryev, T.S. Mikhailova. *J. Alloys. Compounds*, **855** (2), 157504 (2021). DOI: 10.1016/j.jallcom.2020.157504
- [24] P.S. Fernández, A. Arenillas, E.G. Calvo, J.A. Menéndez, M.E. Martins. *Int. J. Hydrogen Energy*, **37**—,(13), 10249 (2012). DOI: 10.1016/j.ijhydene.2012.01.154
- [25] E.H. Lahrar, P. Simon, C. Merlet. *The J. Chem. Ph.*, **155** (18), 184703 (2021). DOI: 10.1063/5.0065150
- [26] M.N. Grigoryev, T.N. Myasoedova, T.S. Mikhailova. *J. Phys. Conf. Ser.*, **1124**, 081043 (2018). DOI: 10.1088/1742-6596/1124/8/081043
- [27] N.K. Plugotarenko, T.N. Myasoedova, M.N. Grigoryev, T.S. Mikhailova. *Nanomaterials*, **9** (12), 1754 (2019). DOI: 10.3390/nano9121754
- [28] F. Stoeckli, T.A. Centeno. *J. Mater. Chem. A*, **1**, 6865 (2013). DOI: 10.1039/c3ta10906b
- [29] M.S. Javed, S. Shoaib, Ahmad Shah, S. Hussain, Sh. Tan, W. Mai. *Chem. Eng. J.*, **382**, 122814 (2020). DOI: 10.1016/j.cej.2019.122814
- [30] X. Zhang, X. Zhang, X. Sun, Y. An, Sh. Song, Ch. Li, K. Wang, F. Su, Ch.-M. Chen, F. Liu, Zh.Sh. Wu, Y. Ma. *J. Power Sources*, **488**, 229454 (2021). DOI: 10.1016/j.jpowsour.2021.229454
- [31] R.K. Kalluri, M.M. Biener, M.E. Suss, M.D. Merrill, M. Stadermann, J.G. Santiago, T.F. Baumann, J. Biener, A. Striolo. *Chem. Phys.*, **15**, 2309 (2013). DOI: 10.1039/C2CP43361C
- [32] J. Jagiello, A. Chojnacka, S.E.M. Pourhosseini, Z. Wang, F. Beguin. *Carbon*, **178**, 113 (2021). DOI: 10.1016/j.carbon.2021.02.098.
- [33] T-Yu. Yi, Ch.-W. Tai, Ch.-Ch. Hu. *J. Power Sources*, **501**, 230029 (2021). DOI: 10.1016/j.jpowsour.2021.230029
- [34] M.D. Stoller, R.S. Ruoff. *Energy Environ. Sci.*, **9**, 1294 (2010). DOI: 10.1039/C0EE00074D
- [35] M.S. Javed, S. Shoaib Ahmad Shah, Sh. Hussain, Sh. Tan, W. Mai. *Chem. Eng. J.*, **382**, 122814 (2020). DOI: 10.1016/j.cej.2019.122814
- [36] D. Cericola, M.E. Spahr. *Electrochim. Acta*, **191**, 558 (2016). DOI: 10.1016/j.electacta.2016.01.121
- [37] N. Devillers, S. Jemei, M.C. Péra, D. Bienaimé, F. Gustin. *J. Power Sources*, **246**, 596 (2014).
- [38] M.E. Suss, Th.F. Baumann, M.A. Worsley, K.A. Rose, Th.F. Jaramillo, M. Stadermann, J.G. Santiago. *J. Power Sources*, **241**, 266 (2013). DOI: 10.1016/j.jpowsour.2013.03.178
- [39] J. Kang, J. Wen, Sh.H. Jayaram, A. Yu, X. Wang. *Electrochim. Acta*, **115**, 587 (2014). DOI: 10.1016/j.electacta.2013.11.002
- [40] J. Kowal, E. Avaroglu, F. Chamekh, A. Šenfělds, T. Thien, D. Wijaya, D.U. Sauer. *J. Power Sources*, **196** (1), 573 (2011). DOI: 10.1016/j.jpowsour.2009.12.028